



Design of microphone phased arrays for acoustic beamforming

Filipe Ramos do Amaral¹ · Juan Carlos Serrano Rico² · Marcello Augusto Faraco de Medeiros¹

Received: 11 November 2017 / Accepted: 18 June 2018 / Published online: 25 June 2018
© The Brazilian Society of Mechanical Sciences and Engineering 2018

Abstract

The design of a microphone array affects the performance of beamforming algorithms in the localization and evaluation of acoustic noise sources. This paper addresses a circular phased array design for near-field aeroacoustic measurements in a closed-test-section wind tunnel. Microphones were distributed in rings and occupied an equal aperture area—each ring could have a different number of microphones. The array performance was evaluated through the dynamic range and array resolution given by the beamwidth. The array designed for the exploration of the novel approach had 112 microphones and 950-mm aperture. In comparison with classical designs, also optimized for the same number of microphones and aperture, the approach provided the best array resolution and a high dynamic range level almost uniform over the frequency range of interest (800 to 20,000 Hz). Microphone shading was also assessed for improving the array performance, and the employment of only the outermost microphones (the innermost ones were shaded) reduced approximately 40% the array beamwidth.

Keywords Aeroacoustics · Microphone phased array design · Acoustic beamforming technique

1 Introduction

Microphone array-based techniques, as beamforming, have become widely spread tools for the study of aeroacoustic noise [11, 16, 22, 28, 32], especially after the development of deconvolution algorithms [5, 10, 15, 33, 37]. Beamforming algorithms steer the microphone array to an assumed distribution of uncorrelated monopole point sources over a region of interest, and they produce a spatial sound pressure level distribution, i.e., a beamforming map. The noise spectra can be calculated by the integration of the sound pressure level distribution for each frequency.

The design of a microphone array is of paramount importance for good beamforming performance. The number of microphones and maximum array aperture, usually limited by the physical space available for their installation, are the main input parameters for the array design. Important performance parameters of the antenna, such as array beamwidth, associated with the spatial resolution of the identified sources, and dynamic range, associated with the maximum side lobe suppression, are provided by the point spread function (PSF). Both parameters are susceptible to optimization by the array distribution of microphones.

Current array designs include circular antennas with microphones distributed over spiral-shaped arrays [3, 9, 14, 23], although multi-arms are also commonly employed [8, 23, 36]. This paper introduces an array design approach for acoustic beamforming, hereinafter called annular, for low- to mid-frequency applications in small closed-test-section wind tunnels. Low- to mid-frequencies must be taken as relative to a reference frequency scale, which, in this case, is given by c / D , where c is the sound speed and D is the array aperture. Variations in sound speed and aperture for a same design modify the optimal frequency range. As the array design was intended for small closed-section wind-tunnel applications, the optimization was conducted only for beamforming in the near-

Technical Editor: André Cavalieri.

✉ Filipe Ramos do Amaral
framal@usp.br

Juan Carlos Serrano Rico
jcserrano@unipamplona.edu.co

Marcello Augusto Faraco de Medeiros
marcello@sc.usp.br

¹ Department of Aeronautical Engineering, University of Sao Paulo, Av. Trabalhador Sao-Carlense, 400., Sao Carlos, SP 13566-590, Brazil

² Programa Ingeniería Mecánica, Universidad de Pamplona, Pamplona, Colombia

field regime, i.e., an acoustic source distance smaller than the array diameter. The performance of the array for far-field sources was not investigated. Low spatial resolution associated with large beamwidth is often a problem for low frequencies. The design focuses on the optimization of the resolution with an acceptable level of dynamic range. In the novel design, the microphones are distributed in annular sections, or rings, and each ring contains a number of microphones chosen by the designer. The area assigned to each microphone is determined from the number of rings, number of microphones for each ring, array aperture and innermost annular section diameter. Accordingly, the internal and external radii of the annular sections are calculated, a rotation is defined among the microphones of each ring and the microphones are distributed over the array. The array design exhibits a plateau-like dynamic range for a given frequency range, owing to the spatial weighting over the array provided by the use of an equal aperture per sensor [23]. The geometry developed was compared with reference antennas designs, and a microphone shading strategy was also explored through the array PSF study and experiments with a loudspeaker.

The paper is organized as follows: Sect. 2 provides a brief literature review of classical antenna approaches employed for acoustic beamforming; Sect. 3 describes the methodology employed, which includes the array performance evaluation parameters, design approach, hardware and experimental setup employed; Sect. 4 reports the results of comparisons among the designed array and other design approaches from the literature and addresses microphone shading applied over the proposed array; and finally, Sect. 5 summarizes the conclusions.

2 Reference designs

Antennas designed for acoustic beamforming are commonly circular, although simpler geometries, such as planar and cross-shaped arrays [18, 19, 30], have also been used for such a purpose. Several proposals have been developed for the optimization of microphone distribution in circular antennas. Spiral array designs are very popular for acoustic beamforming applications, as they ensure a non-redundant spacing among microphones and improve the dynamic range associated with spatial aliasing. The Archimedean spiral array [23] employs a simple spiral formulation, and the designer chooses the maximum and minimum spiral radii and number of spiral turns.

An important step for the microphone array design development was the control of the microphone distribution along the spiral. Dougherty [9] introduced the Dougherty logarithmic spiral, through which microphones are placed into equally spaced arc lengths and more evenly

spaced than the designs described above. The designer selects the maximum and minimum spiral radii and a constant angle between an arc length and the spiral radius corresponding to the microphone position. Arcondoulis et al. [3] aimed at an array with a higher concentration of microphones near the array center and proposed an exponential spiral equation in which the designer chooses the number of spiral turns and four coefficients to set the array size and spacing among the microphones.

The combination of spirals was also another important step for the antenna design. According to multi-arm array design approaches, microphones are evenly distributed among arms. In the Dougherty multi-spiral design [23], each arm is a logarithmic spiral based on Dougherty logarithmic spiral [9] and the arms are evenly distributed around the array center. The designer controls the maximum and minimum spiral radii, number of spiral arms, number of microphones per arm and spiral angle. The spiral arm approach led to other interesting possibilities. Christensen and Hald [7, 8] introduced the Brüel & Kjaer multi-arm design for facilitating the antenna assembling. The microphones are arranged into spokes fixed on two hoops (as in a bicycle wheel), which limit the spoke length. The approach enables a non-uniform microphone spacing along the spokes, and the designer specifies the spoke length, spoke angle and number of microphones per spoke. The array performance is marginally reduced in comparison with the more general multi-spiral strategy and facilitates the use and transport of the antenna. The Underbrink multi-spiral [23, 36] is an evolution of the multi-spiral design and ensures the microphones occupy an equal aperture area over the array. Its design includes the same parameters of the Dougherty multi-spiral array.

Prime and Doolan [29] conducted a comparative study of several antenna geometries for beamforming. According to the results, the multiple spiral arms with evenly spaced microphones provide the best array resolution within an acceptable dynamic range. The concentration of microphones in the array center enhances the dynamic range; however, it reduces the array resolution. The authors concluded the array design proposed by Underbrink [36] with a constant area per microphone offered the best overall performance. Humphreys et al. [17] combined two different and complementary arrays, namely LADA—Large Aperture Directional Array and SADA—Small Aperture Directional Array. The former provides higher resolution noise source maps, whereas the latter yields a better localization of sources for selected noise source regions.

Section 4.1 addresses a performance comparison among our array design, introduced in Sect. 3.2, and six reference antennas designs, namely Archimedean spiral [14, 23], Dougherty logarithmic spiral [9], Arcondoulis spiral [3], Underbrink multi-spiral [36], Brüel & Kjaer multi-arm

[7, 8], described in the above paragraphs. The reference antennas were designed after a brief parametric study based on a sensibility study, not reported here; the best array performance was selected according to an acceptable commitment between the beamwidth and dynamic range criteria, i.e., low beamwidth and high dynamic range values in the 800 Hz to 20 kHz frequency range.

3 Methodology

3.1 Array performance evaluation

The point spread function (PSF) shows the array response to a point source of unitary amplitude, which constitutes a sound pressure level distribution on a plane parallel to the array at a certain distance from it [4, 19, 23]. For the PSF calculation, a mesh of N focal points is defined on the evaluation plane and the array is steered to each focal point at the frequencies of interest according to

$$psf(n, \omega) = \left| \frac{\mathbf{G}_n \mathbf{G}_t^*}{\|\mathbf{G}_n\| \|\mathbf{G}_t\|} \right|^2 \tag{1}$$

where ω is the angular frequency, n is a mesh point and $*$ indicates conjugate transposition. \mathbf{G}_n is a vector containing the transfer function between each microphone and mesh point and \mathbf{G}_t is a vector containing the transfer function between a microphone and target point t , i.e., the mesh point in which the synthetic monopole source is situated. The vector elements are given by

$$G_n(r_{m,n}, \omega) = \frac{e^{-j\omega r_{m,n}/c}}{4\pi r_{m,n}} \tag{2}$$

$$G_t(r_{m,t}, \omega) = \frac{e^{-j\omega r_{m,t}/c}}{4\pi r_{m,t}} \tag{3}$$

where $\mathbf{r}_{m,t}$ is the vector (and $r_{m,t}$ its modulus) containing the m -th microphone position relative to the target point, t , $\mathbf{r}_{m,n}$ is the vector (and $r_{m,n}$ its modulus) containing the m -th microphone position relative to the mesh point n , as shown in Fig. 1, c is the sound speed and j is $\sqrt{-1}$.

As the array aperture is finite and the signal spatial sampling is discrete, the array response pattern, i.e., PSF, shows a wide main lobe surrounded by irregularly distributed sidelobes. Figure 2 shows a schema of a PSF cross section whose main lobe and some sidelobes are visible. The beamwidth is given by the main lobe diameter measured 3 dB below its peak, and the dynamic range is evaluated as the difference between the main lobe peak and the highest sidelobe peak.

The lower the frequency, the wider the beamwidth, hence, the lower the spatial resolution of the acoustic

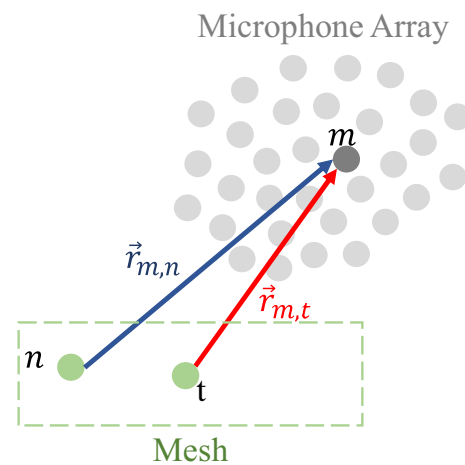


Fig. 1 Diagram of the point spread function (PSF) calculation

sources reconstructed, i.e., even when punctual, the acoustic sources are represented as spots of finite diameter. At higher frequencies, a small beamwidth is achieved and the beamforming algorithms can represent more localized sources. This study considered the 1/12 octave middle frequencies in the 800 Hz to 20 kHz frequency range comprising 56 discrete values.

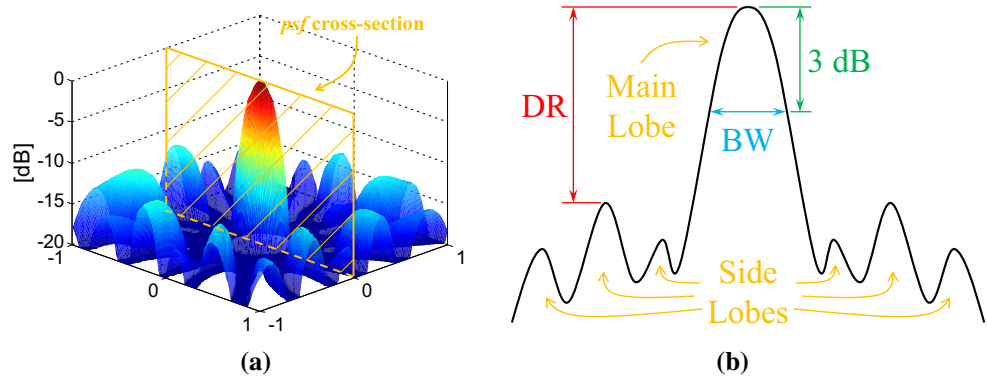
A least square power law fitting was proposed by Brooks and Humphreys [5] as

$$BW(f) \cong C_{BW} \frac{h}{D} f^{-1} \tag{4}$$

where BW is the array beamwidth, h is the distance between the array and beamwidth evaluation mesh plans, D is the array aperture, f is the frequency and C_{BW} is a coefficient that characterizes the array beamwidth at all frequencies and enables the comparison of different microphone arrays. The lower the C_{BW} value, the lower the beamwidth. Such a parameter will be employed in the comparison of the beamwidth performance of the different arrays reported in Sect. 4.

The dynamic range is a highly irregular function of the frequency and strongly dependent on the microphone arrangement. The limited array dynamic range becomes more evident at higher frequencies, as the PSF shows a large number of sidelobes surrounding its main lobe. Sidelobes are considered a problem, as they can be mistaken by additional sources. Owing to their highly irregular distribution over a frequency range of interest, the establishment of a single dynamic range performance parameter is a difficult task. The mean dynamic range is not a sufficient measure because the dynamic range above certain values, say 20 dB, at some frequencies, offers no practical benefit and does not compensate for very low dynamic range values at other frequencies. Therefore, both mean dynamic range (\overline{DR}) and standard deviation (DR_σ) were

Fig. 2 Beamwidth and dynamic range definitions. **a** PSF three-dimensional diagram. **b** PSF two-dimensional diagram



evaluated for the 1/12 octave central frequencies of interest for the evaluation of the dynamic range of the array designs discussed in Sect. 4. A good dynamic range performance combines a high arithmetic mean, i.e., high level, with a low dispersion, i.e., low standard deviation.

For the verification of our codes and procedures, we performed a comparison between our beamwidth and dynamic range estimates for the large aperture directional array (LADA), presented in Humphreys et al. [17], with the estimates given in the publication, Fig. 3. The PSF was evaluated on a plane 1219 mm distant from the array for a $1219 \times 1219 \text{ mm}^2$ mesh size. Humphreys et al. [17] do not provide a dynamic range curve, but only PSF cuts, showing main lobe and some sidelobes, at 6 and 10 kHz frequencies, similar to the scheme of Fig. 2. From the PSF cuts, we estimated the LADA dynamic range values at 6 and 10 kHz as 7.5 dB each. These results and our dynamic range estimates for the LADA are compared in Fig. 3b. The agreement in both beamwidth, Fig. 3a, and dynamic range, Fig. 3b, is very good.

3.2 Design approach

As pointed out by Prime and Doolan [29], the multi-spiral arms proposed by Underbrink [36] provided the best performance among the arrays studied. Nevertheless, the

multi-spiral arms are still somewhat restrictive, as the number of microphones per ring is equal to the number of arms. Here, we investigate improvements to be achieved if such a restriction is relaxed. One a priori benefit is the number of microphones does not need to be a multiple of the number of arms. Yet, the design is based on Underbrink [36] strategy, which maintained an equal aperture area per microphone and substantially improved the dynamic range. Figure 4 shows a diagram of the parameters of the array design strategy proposed.

The designer chooses a number of parameters, namely array aperture, D , first microphone ring diameter, d , total number of rings, Q , and number of microphones per ring, C_q . M is total number of microphones, i.e.,

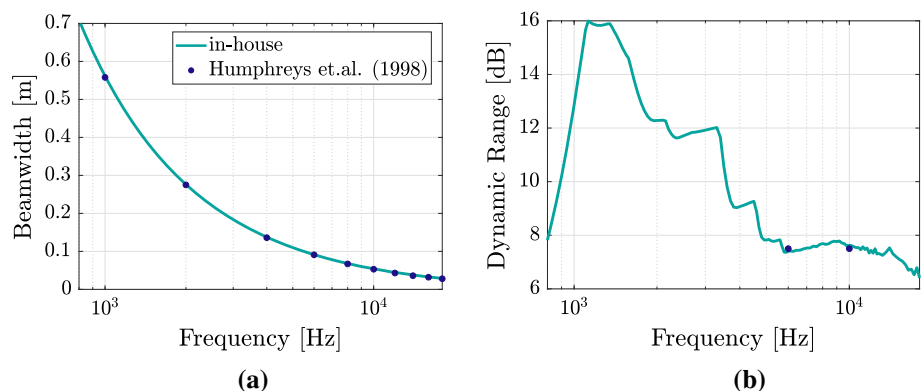
$$M = \sum_{q=1}^Q C_q. \tag{5}$$

For $2 \leq q \leq Q$, the array area subtracted the internal disk area is divided by the total number of microphones minus those of the inner disk, for the evaluation of the area of each microphone, $S_{mic,q \geq 2}$

$$S_{mic,q \geq 2} = \frac{\pi(D^2 - d^2)}{4(M - C_1)} \tag{6}$$

The area of each ring is given by

Fig. 3 LADA beamwidth and dynamic range results. **a** Beamwidth. **b** Dynamic range



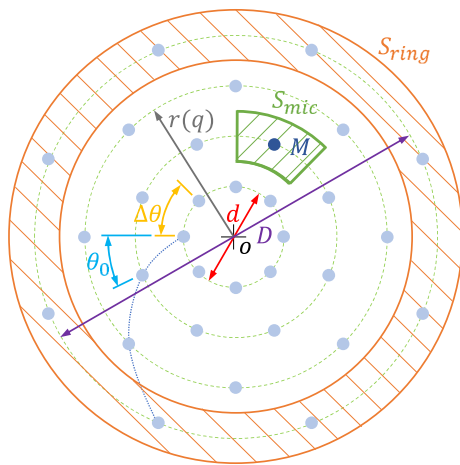


Fig. 4 Diagram of the main parameters of the array design strategy proposed

$$S_q = S_{mic,q \geq 2} C_q \tag{7}$$

for $2 \leq q \leq Q$. The area of the inner disk, i.e., for $q = 1$, is

$$S_1 = \frac{\pi d^2}{4} \tag{8}$$

The microphone radial positions are evaluated through the following recurrence relation

$$r_q = \sqrt{r_{q-1}^2 + \frac{S_q}{\pi}} \tag{9}$$

for $2 \leq q \leq Q$. Note $r_1 = \frac{d}{2}$.

For each array ring, an offset angle, $\theta_{0,q}$, is defined as

$$\theta_{0,q} = (q - 1) \frac{2\pi}{Q} + \theta_{0,1} \tag{10}$$

for $2 \leq q \leq Q$. We chose $\theta_{0,1} = 0$ for the first ring of the current array.

The microphones within each ring have an angular spacing

$$\Delta\theta_q = \frac{2\pi}{C_q} \tag{11}$$

The angle $\theta_{q,m}$, for each microphone of each ring, is then given by

$$\theta_{q,m} = (m - 1)\Delta\theta_q + \theta_{0,q} \tag{12}$$

In cylindrical coordinates, the array microphone positions are r_q and $\theta_{q,m}$.

If a microphone array with all microphones occupying a same aperture area is desired, d should be defined as

$$d = D \sqrt{\frac{C_1}{M}} \tag{13}$$

However, d must be an adjustable parameter defined by the designer. The innermost microphone ring diameter strongly impacts the array dynamic range, as the smaller the diameter d , the higher the dynamic range. On the other hand, a higher d promotes a smaller beamwidth. The innermost microphone ring diameter may also need to be adjusted owing to installation constraints.

3.3 Experimental apparatus

The array is intended for the Low Acoustic Noise and Turbulence (LANT) wind tunnel designed for aeroacoustic and boundary layer research at the University of Sao Paulo, Sao Carlos School of Engineering (USP-EESC) [31]. Its closed test section is 1000 mm high, 1000 mm wide and 3000 mm long, and the microphone array is mounted on the wind-tunnel test-section wall, Fig. 5. Therefore, the array aperture of a circular array could not be larger than 1000 mm and a 950-mm aperture was chosen.

The acoustic instrumentation included a National Instruments acquisition system, which houses up to 112 microphone channels divided into seven PXI-4496 boards of 24-bit 16 analogical inputs. Each PXI-4496 board, which includes built-in anti-aliasing filters, is arranged into a PXI-1042Q chassis and enables the simultaneous sampling of data at rates up to 204.8 kS/s per channel, in a 114 dB dynamic range. Data are transferred at 132 MB/s by the PXI-PCI8336 modulus, which connects the PXI-1042Q chassis and the PXI-8351 computer. 112 G.R.A.S. Sound and Vibration 1/4 in. 40PH microphones are available for the antenna. They reach frequencies of up to 20 kHz and have a large dynamic range of approximately 135 dB. Each microphone contains an integrated CCP preamplifier and built-in TEDS chip. A 4 mA constant current power supply is required for the operation of each microphone.

Tests with a Pioneer TS-MR2040 loudspeaker, employed as an approximation to a monopole source, and an anechoic enclosure, for the avoidance of possible wall, floor and ceiling sound reflections on the microphones flush mounted on the antenna were conducted, Sect. 4.2. A house of foam employed emulated an anechoic enclosure, and its walls were coated with a 100-mm-thick convoluted melamine foam of 0.90 noise reduction coefficient, Fig. 6. The house of foam has internal dimensions of 1000 mm height, 1000 mm width and 900 mm depth, and the antenna is positioned at the loudspeaker opposite wall. The loudspeaker was aligned with the array plane central point and driven by white noise between 20 and 20,000 Hz. The noise emitted by the speaker was acquired by the 112-microphone array at a 48 kHz sampling rate over 20 s.

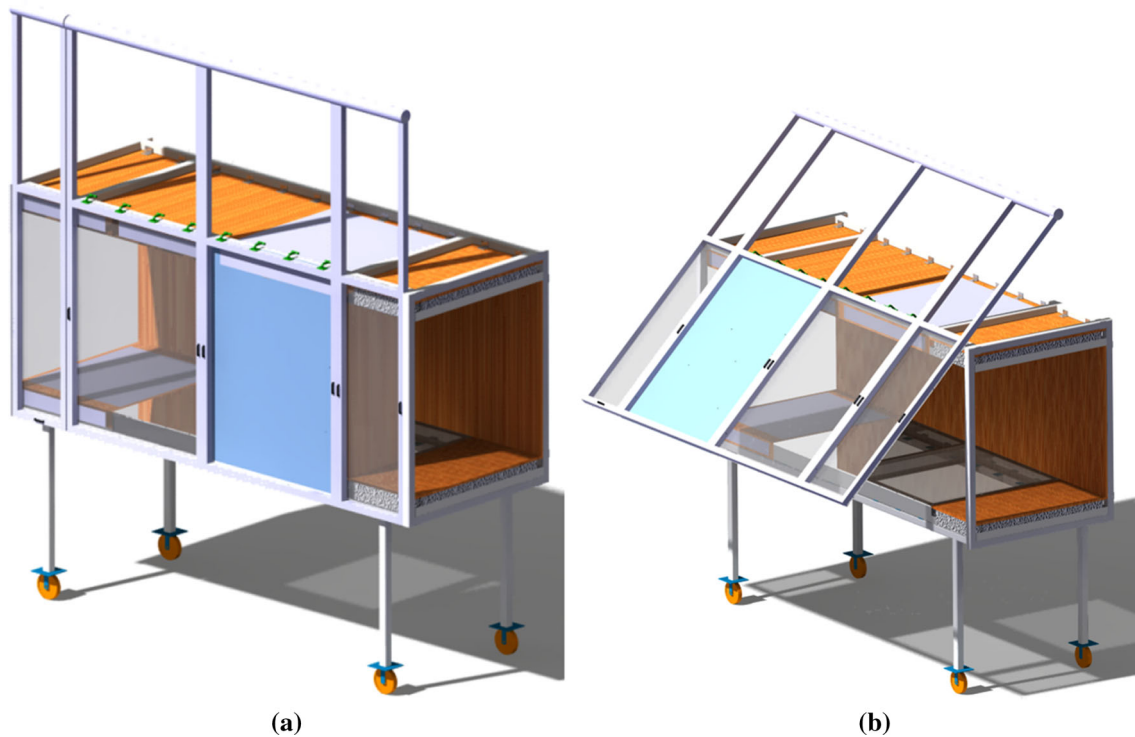


Fig. 5 Test section of the low-speed low-turbulence wind tunnel. The shaded window represents the antenna mounting on the test section



Fig. 6 House of foam employed for experimental cases

4 Results

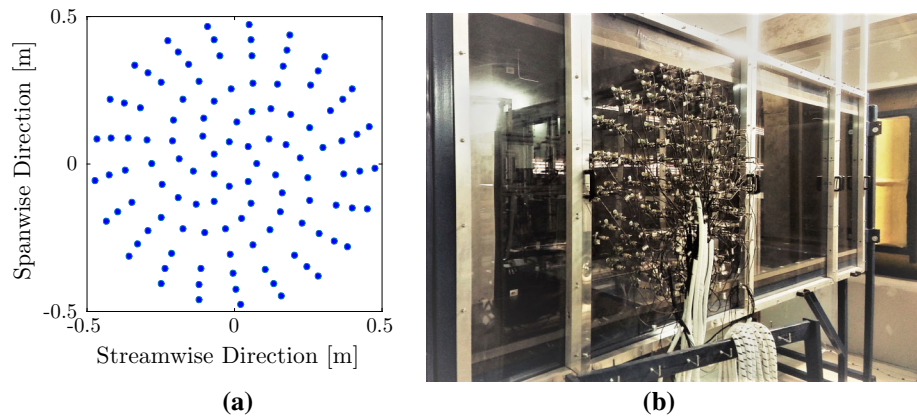
4.1 Comparison among the proposed array and classical designs

A parametric study of the proposed design strategy led to the array shown in Fig. 7a. It employed 112 microphones, which reflects an acquisition system with seven slots with 16 channels each. The microphones were divided into $Q = 10$ rings; each of the seven innermost rings contains seven microphones, and each of the three outermost rings contains 21 microphones. A higher concentration of microphones over the outermost rings was employed, so that

lower beamwidth values could be achieved, whereas the microphone distribution on the other rings ensures an acceptable dynamic range level almost constant in the frequency range of interest. Both array aperture, D , and first ring diameter, d , were chosen as 950 mm (1000 mm is the height of the wind-tunnel test-section walls) and 150 mm, respectively. The optimization procedure was based on a sensitivity study. The number of parameters is vast, the calculations can be time-consuming and some parameters are discrete; therefore, the application of an optimization algorithm can be difficult and we choose to apply a manual optimization procedure. The array aperture and number of microphones were pre-defined due to a well-defined setup and application. Since the goal was not to find the best possible array, but rather, an array design that, for our interest, could be better than the alternatives, the sensitivity analysis, which could be automatized, was sufficient to provide the trends and pointed to some saturation regions. The same approach was employed to optimize the classical designs.

Figure 7b shows a photograph of the antenna rear view mounted on the wind-tunnel test-section wall. The antenna is assembled in a Plexiglas panel of 10 mm thickness and supported in aluminum frames, and the 112 microphones employed in the array are flush mounted. Therefore, the array is essentially mounted flush to an infinite baffle and the Green function is doubled to account for this effect [12]. Such a pressure doubling approximation is correct if

Fig. 7 Antenna design with seven inner rings containing seven microphones each and three outer rings containing 21 microphones each, which total 112 microphones. **a** Microphone positions of the designed antenna. **b** Antenna mounted on the wind-tunnel test section



the acoustic wavelength is significantly smaller than the array aperture. If the acoustic wavelength is comparable or larger than the array aperture, it can be important to consider diffraction or reverberation effects [11, 20, 35]. Such effects are not considered in our beamforming codes and are generally not considered in beamforming codes used in closed-test-section wind tunnel experiments [13, 21, 24, 25]. It is admitted that the approach may be inadequate for low frequencies, but based on the literature [12] and on a previous work in which our experimental beamforming results were compared with numerical simulation results of slat noise [26], we expect the beamforming approach here described would be satisfactory above 800 Hz frequency. It is also noted that the wind tunnel for which this array is intended has provision for acoustic treatment on the working section walls, which, as shown in Serrano Rico et al. [31], reduce significantly these effects.

Figure 8 shows the PSF of the designed array for 1, 2, 4, 8 and 16 kHz frequencies, from which both beamwidth and dynamic range data were extracted. Note the side lobes distribution around the main peak shows a remarkably good circular symmetry that is normally taken as a good indication [23].

Comparisons were carried out with some classical reference designs with the performance parameters formerly described for accessing the benefits of the annular design. Figure 9 shows six reference classical antenna designs for comparisons with the array design approach introduced in Sect. 3.2. All antennas were designed with 112 microphones and $D = 950$ mm aperture and optimized to a substantial degree.

Figure 10 displays the array performance results of the classical antenna designs (Fig. 9) and those of the annular antenna for the 1/12 octave frequencies within the 800 to 20,000 Hz range. More quantitative results are found in Table 1, which shows the array performance evaluation coefficients defined in Sect. 3.1 and Eq. 4 for the different antennas studied. The array PSF was evaluated on a plane

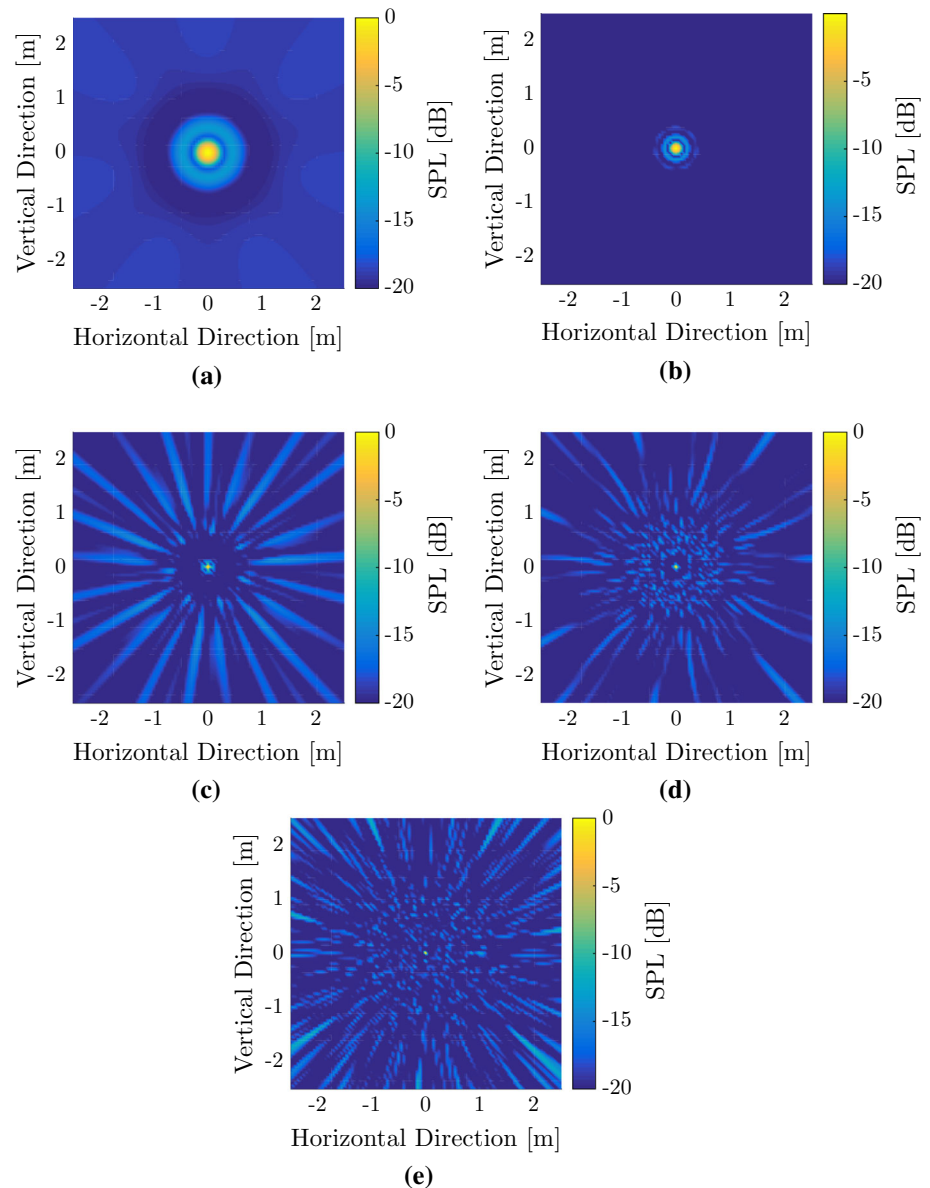
500 mm distant from the array for a 5000×5000 mm² mesh size with 10 mm equally spaced points, which resulted in 251,001 discrete points for each frequency of interest. For lower frequencies, the PSF shows only a single wide main lobe in the mesh used; therefore, the dynamic range results are less reliable.

The proposed design approach (annular) exhibited the lowest beamwidth values among all designs, i.e., approximately 300 mm at 800 Hz and C_{BW} of 459.9579 m/Hz, followed by Underbrink multi-spiral (320 mm at 800 Hz, C_{BW} of 484.0305 m/Hz) and Dougherty spiral (340 mm at 800 Hz, C_{BW} of 504.6835 m/Hz). Arcondoulis spiral showed the worst beamwidth performance, i.e., approximately 470 mm at 800 Hz and C_{BW} of 694.1238 m/Hz—remember C_{BW} parameter was defined in Eq. 4, Sect. 3.1. The Archimedean spiral geometry exhibited the best dynamic range levels, i.e., the highest \overline{DR} , followed by the Arcondoulis spiral geometry. However, the antennas of best \overline{DR} performance coefficient did not display a similar dynamic range performance in the frequency range, i.e., such designs exhibit high DR_{σ} values, Table 1, owing to the higher dynamic range values at lower frequencies, Fig. 10. For instance, they can reach a dynamic range well above 20, which is certainly unnecessary for most applications. The Underbrink multi-spiral and Dougherty spiral approaches do not show such a large \overline{DR} ; however, their dynamic ranges are more evenly spread throughout the spectrum, i.e., the designs show low DR_{σ} values.

Overall, the results convey the underlying concept that a higher dynamic range and a smaller beamwidth are conflicting demands. Interestingly, the annular design provided the smallest beamwidth (C_{BW}), the lowest DR_{σ} and an acceptable \overline{DR} level, hence, a good balance between such conflicting requirements with a fairly constant dynamic range level throughout the frequency range.

Figure 11 shows an assessment of the beamwidth and dynamic range performance degradation over a line in the horizontal direction for the annular array. The PSF curves

Fig. 8 Annular array PSF for selected frequencies. **a** 1 kHz. **b** 2 kHz. **c** 4 kHz. **d** 8 kHz. **e** 16 kHz



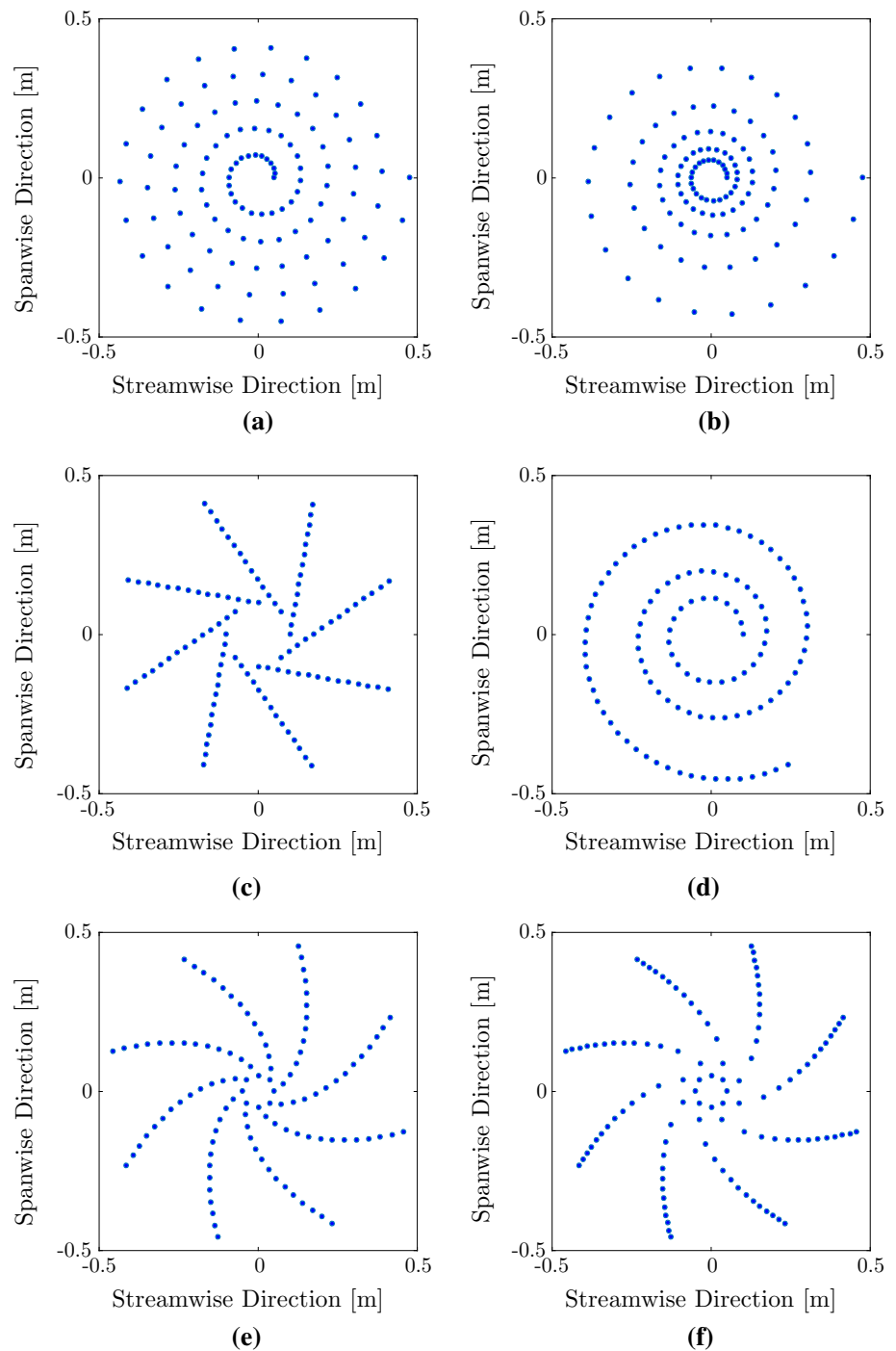
were evaluated for a punctual monopole source at several target points between $(x_t, y_t, z_t) = (-475, 0, 500)$ and $(475, 0, 500)$ mm. A source horizontally and vertically centered on the array shows the best combined performance, i.e., higher C_{BW} and \overline{DR} , and acceptable DR_σ . The C_{BW} performance is essentially symmetrical with respect to the microphone array center. Such a symmetry is not observed for the dynamic range parameter performance. In general, the dynamic range shows a degradation trend with the source moving from the array center. The trends along a vertical line are similar to those of the horizontal line, in particular for the beamwidth. Johnson and Dudgeon [19], Mueller et al. [23] and Prime and Doolan [29] reported degradations in both beamwidth and dynamic range for sources far from the array center. The level of degradation

observed in the current design can be considered similar to that of other designs, i.e., the proposed design does not overcome or circumvent those degradation tendencies and is not more vulnerable to such effects than other designs.

4.2 Improvement in array performance by shading

Array shading is a common acoustic beamforming practice [2, 6, 34]. One of the array shading approaches employs only a portion of the microphones composing the antenna. The performance of several antenna configurations comprised of selected rings, i.e., 1–7 (configuration #1, 49 microphones), 1–3 and 9–10 (configuration #2, 63 microphones), 5–7 and 9–10 (configuration #3, 63 microphones),

Fig. 9 Antennas designed according to the reference strategies. **a** Archimedes spiral. **b** Arcondoulis spiral. **c** Brüel & Kjaer multi-arm. **d** Dougherty spiral. **e** Dougherty multi-spiral. **f** Underbrink multi-spiral



8–10 (configuration #4, 63 microphones) and 1–10 (configuration #0, 112 microphones, full array) was evaluated regarding beamwidth and dynamic range.

Figure 12 and Table 2 show, respectively, array performance parameters and their coefficients. The analysis indicates the use of only the outer array microphones can reduce the beamwidth. Configuration #4, which employed the outermost microphones, displays the lowest beamwidth values, for example, approximately 250 mm at 800 Hz, and

C_{BW} of 376.5635. The trade-off alluded corresponds to a reduction in both beamwidth and dynamic range. Yet, the dynamic range distribution over the frequency of interest remained uniform.

Experiments with a loudspeaker positioned near the array center in a plane 900 mm apart from the array, Sect. 3.3, were performed for illustrating the array shading effect over the beamforming map. The array used was based on the proposed design, i.e., the annular array. In-

Fig. 10 Performance evaluation parameters of reference strategy antennas for 800 to 20,000 Hz 1/12 octave frequency range. **a** Beamwidth. **b** Dynamic range

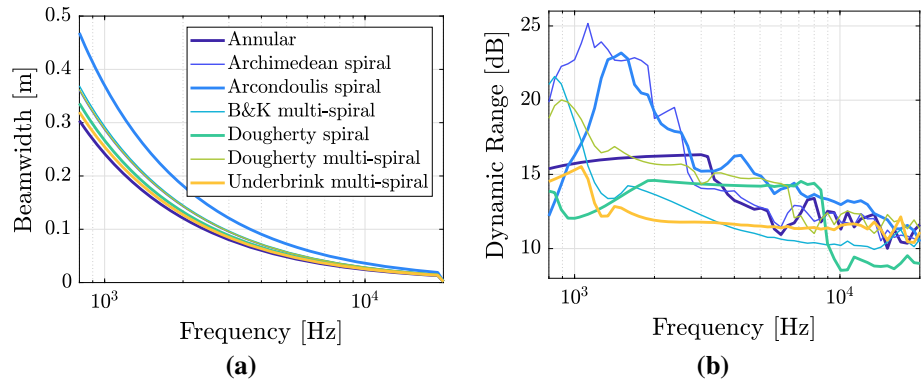


Table 1 Beamwidth and dynamic range performance coefficients of reference strategy antennas evaluated for 800 to 20,000 Hz 1/12 octave frequency range

Array	C_{BW} (m/Hz)	\overline{DR} (dB)	DR_{σ} (dB)
Annular	459.9579	13.9579	2.0116
Archimedean spiral	542.6654	15.6935	4.6362
Arcondoulis spiral	694.1238	14.8299	3.8398
B&K multi-spiral	553.1658	12.9228	3.0458
Dougherty spiral	504.6835	12.6359	2.1276
Dougherty multi-spiral	546.0115	14.5404	2.4281
Underbrink multi-spiral	484.0305	12.2647	1.2575

Annular design results are given for reference

house beamforming algorithms [1, 2, 26, 27] were employed for the signal post-processing. For the calculations of the beamforming maps, the mesh was contained in a squared domain of 1500×1500 mm minimum dimensions with 10 mm equally spaced points; it was centered in the array 900 mm apart from the array plan, i.e., the same distance within which the loudspeaker was positioned. Figures 13 and 14 show the conventional beamforming maps for the five different array shadings presented above and 800 and 2250 Hz frequencies. Only sound pressure levels 12 dB below the peak normalized for exhibiting a 0 dB maximum value are displayed. A cross indicates the loudspeaker source position in the figures.

Fig. 11 Study of the annular microphone array beamwidth and dynamic range performance degradation. **a** Beamwidth. **b** Dynamic range

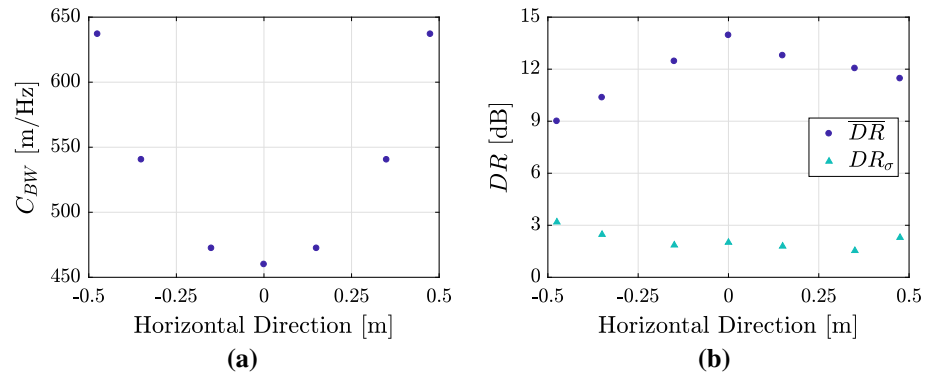


Fig. 12 Parameters of performance evaluation of different array configurations / shading for 800 Hz to 20 kHz 1/12 octave frequency range. **a** Beamwidth. **b** Dynamic range

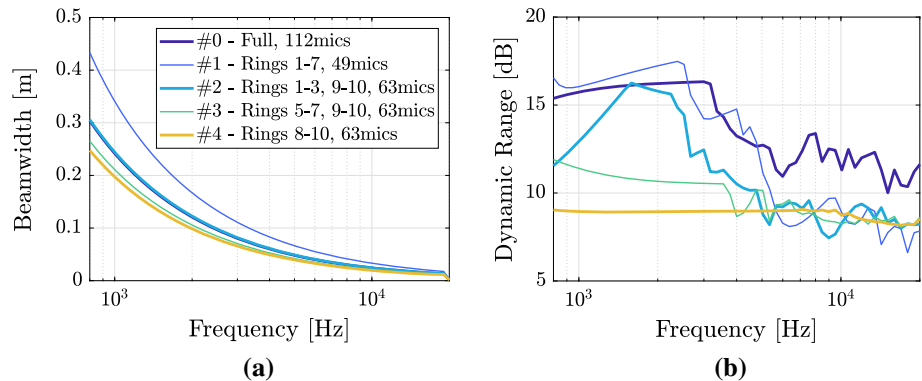
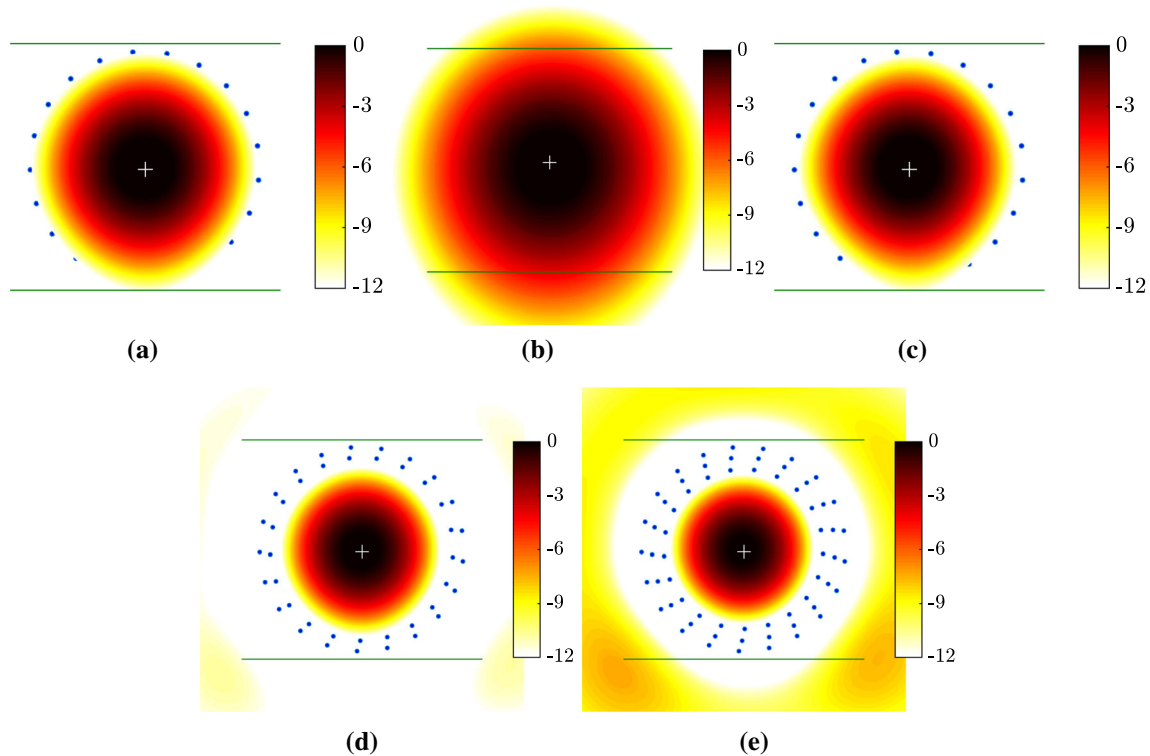


Table 2 Performance coefficients of array microphone shading configurations evaluated for 1/12 octave frequency within the 800 to 20,000 Hz range

Array	C_{BW} (m/Hz)	\overline{DR} (dB)	DR_{σ} (dB)
#0-Full, 112 microphones	459.9579	13.9579	2.0116
#1-Rings 1–7, 49 microphones	637.7129	12.9567	3.7815
#2-Rings 1–3, 9–10, 63 microphones	466.5477	11.1957	2.6796
#3-Rings 5–7, 9–10, 63 microphones	402.5416	10.0774	1.3784
#4-Rings 8–10, 63 microphones	376.5635	8.8790	0.2618

**Fig. 13** Conventional beamforming acoustic maps of a speaker source at 800 Hz for different array shadings. **a** #0, Full. **b** #1, 1–7. **c** #2, 1–3 and 9–10. **d** #3, 5–7 and 9–10. **e** #4, 8–10

The acoustic map for microphones distributed near the array center, as in configuration #1, Fig. 14, shows a wider source in comparison with the full array. On the other hand, configurations #3 and #4, which use an outer microphone distribution, display acoustic maps with a narrower source representation, although a number of sidelobes surround the noise. In view of the results from the full array, the determination of the real source is not ambiguous and the source localization is substantially better. Under some circumstances, a strategy using the external microphones via shading may improve the source localization of previously isolated sources through the use of a full array, which can be useful for investigations on low-frequency noise sources in small wind tunnels.

5 Conclusions

This paper has introduced a microphone phased array design approach for near-field acoustic beamforming. A total of 112 microphones were distributed over a 950-mm aperture representing a setup for a closed-test-section wind tunnel. Beamwidth and dynamic range parameters, defined through the array PSF, were employed for the evaluation of the array performance. A good microphone array design combines a small beamwidth and a high dynamic range; however, the achievement of good performance in both items simultaneously is difficult.

The annular design combined the characteristics of the Underbrink multi-spiral array, i.e., an equal aperture area per microphone guided by a reference spiral, with the possibility of more microphones distributed over the outermost rings, which enhanced the array resolution (low

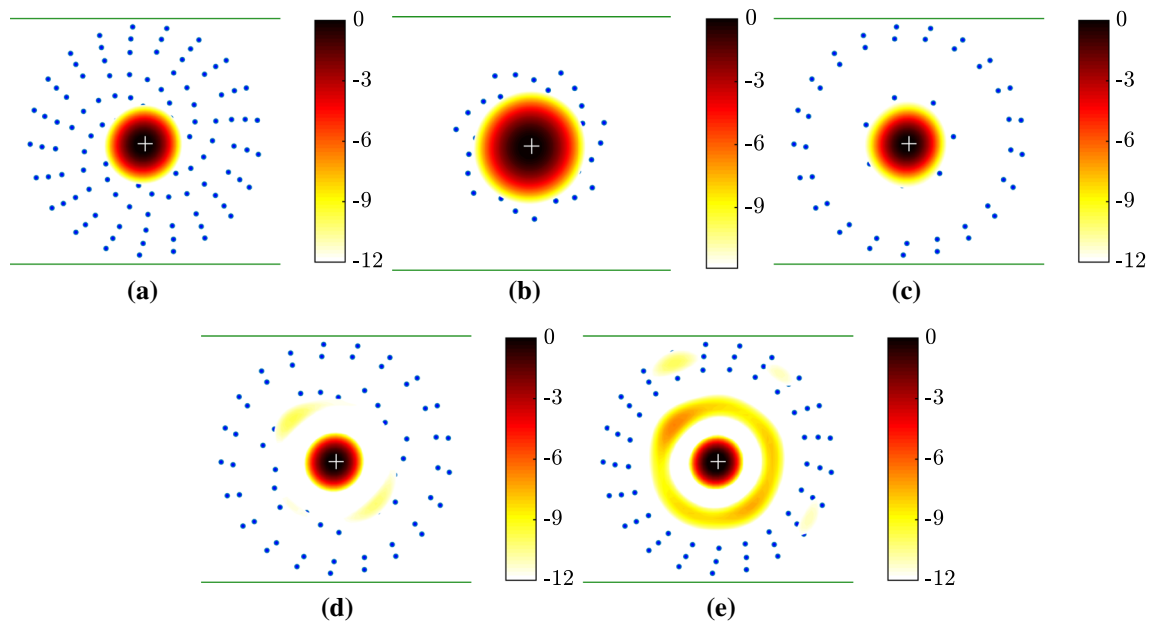


Fig. 14 Conventional beamforming acoustic maps of a loudspeaker source at 2,250 Hz for different array shadings. **a** #0, Full. **b** #1, 1–7. **c** #2, 1–3 and 9–10. **d** #3, 5–7 and 9–10. **e** #4, 8–10

beamwidth). The beamwidth requires special attention for small closed-test-section wind tunnels, as the noise source evaluation plan is very close to the microphone array. Comparisons with reference design strategies revealed the proposed array exhibits the lowest beamwidth, whereas a very high averaged dynamic range was achieved with an even distribution over the frequency range of interest. The performance degradation for a source located far from the array center is similar to that observed in other designs. A design with a high concentration of microphones near the array aperture and a moderate concentration over its center provided the best balance between the beamwidth and dynamic range for our current interests. The idea, however, can be applied, within limits, for the control of such parameters.

A study of possible array configurations produced by microphone shading was also carried out. When the 63 outermost array microphones were used, a 40% beamwidth improvement was achieved at an expense of an approximately 35% reduction in the dynamic range mean level. For beamforming purposes, a combination of the full array and microphone shading schemes can be employed for the association of a good level quantification (full array) and better source localization (outer microphone rings).

Acknowledgements F.R.A. received funding from Coordination for the Improvement of Higher Education Personnel (CAPES/Brazil), Grant #DS00011/07-0. J.C.S.R. received support from National Council for Scientific and Technological Development (CNPq/Brazil), Grant #140211/2014-4. M.A.F.M. received support from CNPq/Brazil, Grant #304859/2016-8. The authors also acknowledge the Sao Paulo Research Foundation (FAPESP/Brazil) and EMBRAER S.A./

Brazil, Grant #2006/52568-7, Funding Authority for Studies and Projects (FINEP/Brazil), Grant #01.09.0334.04, for their financial support, Mr. Christian Salaro Bresci and Mr. Matheus Maia Beraldo, for their technical support with the loudspeaker experiment and Mrs. Angela Giampetro for her support with the scientific writing.

References

1. Amaral FR, Souza DS, Pagani CC Jr, Himeno FHT, Medeiros MAF (2015) Experimental study of the effect of a small 2d excrescence placed on the slat cove surface of an airfoil on its acoustic noise. In: 21st AIAA/CEAS aeroacoustics conference, p 3138. <https://doi.org/10.2514/6.2015-3138>
2. Amaral FR, Himeno FHT, Pagani CC Jr, Medeiros MAF (2018) Slat noise from an md30p30n airfoil at extreme angles of attack. *AIAA J* 56(3):964–978. <https://doi.org/10.2514/1.J056113>
3. Arcondoulis EJG, Doolan CJ, Zander AC, Brooks LA (2010) Design and calibration of a small aeroacoustic beamformer. In: Proceedings of the 20th international congress on acoustics, international congress on acoustics, p 8. URL http://www.acoustics.asn.au/conference_proceedings/ICA2010/cdrom-ICA2010/papers/p453.pdf
4. Benesty J, Sondhi M, Huang Y (2008) Microphone array signal processing. Springer, Berlin, Germany
5. Brooks TF, Humphreys WM (2006) A deconvolution approach for the mapping of acoustic sources (damas) determined from phased microphone arrays. *J Sound Vib* 294(4–5):856–879. <https://doi.org/10.1016/j.jsv.2005.12.046>
6. Brooks TF, Humphreys WM, Plassman GE (2010) Damas processing for a phased array study in the nasa langley jet noise laboratory. In: 16th AIAA/CEAS aeroacoustics conference, p 3780. <https://doi.org/10.2514/6.2010-3780>
7. Christensen JJ, Hald J (2004) Technical review: beamforming. Report. Briel & Kjaer, Naerum, Denmark
8. Christensen JJ, Hald J (2006) Beam forming array of transducers. US Patent 7,098,865

9. Dougherty RP (1998) Spiral-shaped array for broadband imaging. US Patent 5,838,284
10. Ehrenfried K, Koop L (2007) Comparison of iterative deconvolution algorithms for the mapping of acoustic sources. *AIAA J* 45(7):1584–1595. <https://doi.org/10.2514/1.26320>
11. Fenech B, Takeda K (2007) Beamforming in highly reverberant wind tunnels possibilities and limitations. In: 14th International congress on sound and vibration (ICSV14), Australian Acoustics Society, pp 1–8. URL <http://eprints.soton.ac.uk/48626/>
12. Fischer J, Doolan C (2017) Improving acoustic beamforming maps in a reverberant environment by modifying the cross-correlation matrix. *J Sound Vib* 411:129–147. <https://doi.org/10.1016/j.jsv.2017.09.006>
13. Fleury V, Bulté J, Davy R, Manoha E, Pott-Pollenske M (2015) 2d high-lift airfoil noise measurements in an aerodynamic wind tunnel. In: 21st AIAA/CEAS aeroacoustics conference, p 2206. <https://doi.org/10.2514/6.2015-2206>
14. Fonseca WD, Ristow JP, Sanches DG, Gerges SNY (2010) A different approach to Archimedean spiral equation in the development of a high frequency array. In: SAE Technical Paper, SAE International, p 10. <https://doi.org/10.4271/2010-36-0541>
15. Herold G, Sarraj E (2015) An approach to estimate the reliability of microphone array methods. In: 21st AIAA/CEAS aeroacoustics conference, American Institute of Aeronautics and Astronautics, p 2977. <https://doi.org/10.2514/6.2015-2977>
16. Huang X, Bai L, Vinogradov I, Peers E (2012) Adaptive beamforming for array signal processing in aeroacoustic measurements. *J Acoust Soc Am* 131(3):2152
17. Humphreys W, Brooks T, Hunter W, Meadows K (1998) Design and use of microphone directional arrays for aeroacoustic measurements. In: 36th AIAA aerospace sciences meeting and exhibit, p 471. <https://doi.org/10.2514/6.1998-471>
18. Jean-François P, Elias G (1997) Airframe noise source localization using a microphone array. In: 3rd AIAA/CEAS aeroacoustics conference, American Institute of Aeronautics and Astronautics, p 1643. <https://doi.org/10.2514/6.1997-1643>
19. Johnson DH, Dudgeon DE (1993) Array signal processing: concepts and techniques. Prentice Hall, New York
20. Kröber S (2013) Comparability of microphone array measurements in open and closed wind tunnels. Ph.D. thesis, Technische Universität Berlin. URL <https://opus4.kobv.de/opus4-tuberlin/frontdoor/index/index/docId/4564>
21. Li L, Liu P, Guo H, Hou Y, Geng X, Wang J (2017) Aeroacoustic measurement of 30p30n high-lift configuration in the test section with Kevlar cloth and perforated plate. *Aerosp Sci Technol* 70:590–599. <https://doi.org/10.1016/j.ast.2017.08.039>
22. Michel U (2006) History of acoustic beamforming. In: 1st Berlin beamforming conference, Berlin beamforming conference, pp 1–17. URL http://elib.dlr.de/47021/1/BeBeC_2006_Paper_Michel.pdf
23. Mueller TJ, Allen CS, Blake WK, Dougherty RP, Lynch D, Soderman PT, Underbrink JR (2002) Aeroacoustic measurements. Springer, Berlin
24. Murayama M, Nakakita K, Yamamoto K, Ura H, Ito Y, Choudhari MM (2014) Experimental study on slat noise from 30p30n three-element high-lift airfoil at jaxa hard-wall lowspeed wind tunnel. In: 20th AIAA/CEAS aeroacoustics conference, AIAA aviation, p 2080. <https://doi.org/10.2514/6.2014-2080>
25. Oerlemans S (2009) Detection of aeroacoustic sound sources on aircraft and wind turbines. Ph.D. thesis, University of Twente. URL <http://citeseerx.ist.psu.edu/viewdoc/download?doi=10.1.1.452.2753&rep=rep1&type=pdf>
26. Pagani CC Jr, Souza DS, Medeiros MAF (2016) Slat noise: aeroacoustic beamforming in closed-section wind tunnel with numerical comparison. *AIAA J* 54(7):2100–2115. <https://doi.org/10.2514/1.J054042>
27. Pagani CC Jr, Souza DS, Medeiros MAF (2017) Experimental investigation on the effect of slat geometrical configurations on aerodynamic noise. *J Sound Vib* 394:256–279. <https://doi.org/10.1016/j.jsv.2017.01.013>
28. Papamoschou D (2011) Imaging of directional distributed noise sources. *J Sound Vib* 330(10):2265–2280. <https://doi.org/10.1016/j.jsv.2010.11.025>
29. Prime Z, Doolan C (2013) A comparison of popular beamforming arrays. In: Proceedings of ACOUSTICS 2013, Australian Acoustical Society, p 7. URL http://www.acoustics.asn.au/conference_proceedings/AAS2013/papers/p5.pdf
30. Pumphrey HC (1993) Design of sparse arrays in one, two, and three dimensions. *J Acoust Soc Am* 93(3):1620–1628. <https://doi.org/10.1121/1.406821>
31. Serrano Rico JC, Amaral FR, Bresci CS, Medeiros MAF (2017) Design of a low-speed, closed test-section wind-tunnel for aeroacoustic and low-turbulence experiments. In: 24th ABCM international congress of mechanical engineering, Associação Brasileira de Engenharia e Ciências Mecânicas, Proceedings of COBEM2017, p 12
32. Shin HC, Graham W, Sijtsma P, Andreou C, Faszer AC (2007) Implementation of a phased microphone array in a closed-section wind tunnel. *AIAA J* 45(12):2897–2909. <https://doi.org/10.2514/1.30378>
33. Sijtsma P (2007) Clean based on spatial source coherence. *Int J Aeroacoust* 6(4):357–374. <https://doi.org/10.1260/147547207783359459>
34. Sijtsma P (2010) Phased array beamforming applied to wind tunnel and fly-over tests. SAE Technical Paper p 22. <https://doi.org/10.4271/2010-36-0514>
35. Sijtsma P, Holthusen H (2003) Corrections for mirror sources in phased array processing techniques. In: 9th AIAA/CEAS aeroacoustics conference, p 3196. <https://doi.org/10.2514/6.2003-3196>
36. Underbrink JR (2001) Circularly symmetric, zero redundancy, planar array having broad frequency range applications. US Patent 6,205,224
37. Yardibi T, Zawodny NS, Bahr C, Liu F, Cattafesta LN, Li JA (2010) Comparison of microphone array processing techniques for aeroacoustic measurements. *Int J Aeroacoust* 9(6):733–761. <https://doi.org/10.1260/1475-472X.9.6.733>